REVIEW

**MENG Jie, GUO Jian-you,
LIU Lang, ZHANG Shuang-quan**

Shell-model-like Approach (SLAP) for the Nuclear Properties in Relativistic Mean Field Theory

Abstract A Shell-model-like approach suggested to treat the pairing correlations in relativistic mean field theory is introduced, in which the occupancies thus obtained have been iterated back into the densities. The formalism and numerical techniques are given in detail. As examples, the ground state properties and low-lying excited states for Ne isotopes are studied. The results thus obtained are compared with the data available. The binding energies, the odd–even staggering, as well as the tendency for the change of the shapes in Ne isotopes are correctly reproduced.

PACS numbers 21.60.Jz, 21.60.Cs, 21.10.Re, 21.10.Dr

1 Introduction

The relativistic mean field (RMF) theory is one of the most successful microscopic models [1]. During the past two decades, it has received wide attention due to its success in describing many nuclear phenomena for the stable nuclei [2,3] as well as nuclei that were far from being stable [4,5]. It has been shown that the relativistic mean field theory can reproduce better the nuclear saturation properties (the Coester line) in nuclear matter [6], present a new explanation for the identical bands in superdeformed nuclei [7] and the neutron halo [8], predict a new phenomenon— giant neutron halos in heavy nuclei close to the neutron

MENG Jie (✉), GUO Jian-you,
LIU Lang, ZHANG Shuang-quan
School of Physics, Peking University,
Beijing 100871, China
E-mail: mengj@pku.edu.cn

MENG Jie
Institute of Theoretical Physics, Chinese Academy of Sciences,
Beijing 100080, China
Center of Theoretical Nuclear Physics,
National Laboratory of Heavy Ion Accelerator,
Lanzhou 730000, China

GUO Jian-you
Department of Physics, Anhui University,
Hefei 230039, China

drip line [9], give naturally the spin–orbit potential, the origin of the pseudospin symmetry [10,11] as a relativistic symmetry [12–14], and spin symmetry in the anti-nucleon spectrum [15], and present a good description for the magnetic rotation [16] and the collective multipole excitations [17], etc.

Pairing correlations play an essential role in nuclear properties such as binding energies, odd–even effects, single particle orbit occupation, electric–magnetic transition, low-lying collective modes, moment of inertia, halo phenomena, etc. The RMF theory must be supplemented with the proper treatment of the pairing correlations to be realistic and to describe the open shell nuclei. This aspect becomes all the more important when considering the continuum effects, which are crucial for the description of drip line nuclei. So far, the most commonly used methods, the Bardeen–Cooper–Schrieffer (BCS) approximation and Bogoliubov transformation, have become standard in nuclear physics literatures [18,19], even for exotic nuclei where the Bogoliubov transformation is required to be done in coordinate space [4,8,20,21] or the introduction of the resonant states is necessary [22–25].

As the approximate product of the quasiparticle wave functions in quasiparticle formalism breaks the gauge symmetries connected with the particle numbers, the projection methods are introduced to restore the broken symmetries [26]. There exist a vast amount of literature on such projection methods (see, for instance, [27] and references therein). The variation after projection (VAP) [28] is the appropriate tool that fulfills the variation principle and provides a self-consistent description of fluctuations going beyond mean field. Although the VAP method has been known for quite a long time, the numerical solution of the corresponding variation equations is relatively complicated. A fully self-consistent variation after exact projection has been carried out so far only in a limited number of cases [27,29]. Exact projection within full HFB theory is possible by a search of the minimum in the projected-energy surface by gradient methods [30]. However, these methods are numerically very complicated and have been applied only to the case of number projection in restricted spaces and for separable forces [31]. The problem whether simple HFB-like equations can be

obtained with the projected energy functional has been recently addressed [32], and it has been shown that the variation of an arbitrary energy functional, which is completely expressed in terms of the HFB density matrix ρ and the pairing tensor κ, results in HFB-like equations with modified expressions for the pairing potential and the Hartree–Fock field [33]. This would allow the usage of numerical algorithms for diagonalization of matrices, as it was carried out in the ordinary HFB theory.

Meanwhile, the defects including the violation of the particle number conservation and improbable treatment for the Pauli blocking effects [34–37] in both the BCS approximation and Bogoliubov transformation for finite fermion system like nuclei can be avoided in the Shell-model-Like APproach (SLAP) [34], which was originally referred as Particle Number Conserving (PNC) method there.

Compared with the complicated particle number projection technique, the SLAP proposed in the 1980s [34] avoids all the difficulties encountered in BCS and Bogoliubov approximation and takes into account the Pauli blocking effects strictly by diagonalizing the pairing Hamiltonian directly in a reasonable configuration space. It has been found that the number of the configurations with important weights in the low-lying solutions is quite limited; only a few lowest-energy configurations contribute significantly [39]. This conclusion has been used as the guideline of a many-body configuration truncation by retaining a certain number of the lowest energy states. Extensive studies and discussion on the validity of the truncated many-body spaces as well as its application can be found in [39–43] and references therein. The application of the SLAP to solve the nuclear mean field plus pairing Hamiltonian problem with a realistic deformed Woods–Saxon single-particle potential has been reported in [38]. The optimal basis construction has been discussed and the stability of the final result with respect to the basis cutoff has been illustrated. In particular, the presence of the low-lying seniority $s = 0$ solutions, which are usually poorly described in terms of the standard BCS or HFB approximation, has been found to play a role in the interpretation of the spectra of rotating nuclei.

As SLAP is based on the direct diagonalization of the pairing Hamiltonian in the multiparticle configuration (MPC) space, it has been shown to be more accurate than the BCS calculation as compared with the exact solution at least for the small systems [38]. Furthermore, the blocking effects are taken into account automatically and both odd–A and even–even nuclei can be treated on the same footing. In addition, the excitation spectrum can be obtained conveniently in the present algorithm.

In this paper, SLAP is suggested to treat the pairing correlations in RMF theory, in which the occupancies thus obtained have been iterated back into the densities. A brief formalism is presented in Section 2. The numerical details and its application for the ground state properties and low-lying excited spectrum for Ne isotopes as well as the comparison with data are given in Section 3. Finally, a brief summary is given in Section 4.

2 Formalism

2.1 RMF theory

In the framework of RMF theory, the nuclear effective interaction is usually described by the exchange of three mesons: the scalar meson σ, which mediates the medium-range attraction between the nucleons, the vector meson ω^μ, which mediates the short-range repulsion, and the isovector–vector meson ρ^μ, which provides the isospin dependence of the nuclear force. The effective Lagrangian density is presented as the following:

$$
\begin{aligned}
\mathcal{L} = &\ \overline{\psi}(\mathrm{i}\gamma^\mu \partial_\mu - M)\psi \ + \ \frac{1}{2}\partial^\mu \sigma \partial_\mu \sigma \ - \ \frac{1}{2}m_\sigma^2 \sigma^2 \\
&- \frac{1}{3}g_2 \sigma^3 \ - \ \frac{1}{4}g_3 \sigma^4 - g_\sigma \overline{\psi}\sigma\psi \ - \ \frac{1}{4}\Omega^{\mu\nu}\Omega_{\mu\nu} \\
&+ \frac{1}{2}m_\omega^2 \omega^\mu \omega_\mu \ - \ g_\omega \overline{\psi}\gamma^\mu \psi \omega_\mu \ + \ \frac{1}{4}g_4(\omega^\mu \omega_\mu)^2 \\
&- \frac{1}{4}\boldsymbol{R}^{\mu\nu}\cdot \boldsymbol{R}_{\mu\nu} \ + \ \frac{1}{2}m_\rho^2 \boldsymbol{\rho}^\mu \cdot \boldsymbol{\rho}_\mu \ - \ g_\rho \overline{\psi}\gamma^\mu \boldsymbol{\tau}\cdot \psi \boldsymbol{\rho}_\mu \\
&- \frac{1}{4}F^{\mu\nu}F_{\mu\nu} \ - \ e\overline{\psi}\gamma^\mu \frac{1-\tau_3}{2}A_\mu \psi
\end{aligned}
\tag{1}
$$

where the field tensors of the vector mesons and the electromagnetic field take the forms:

$$
\begin{cases}
\Omega^{\mu\nu} \ = \ \partial^\mu \omega^\nu \ - \ \partial^\nu \omega^\mu \\
\boldsymbol{R}^{\mu\nu} \ = \ \partial^\mu \boldsymbol{\rho}^\nu \ - \ \partial^\nu \boldsymbol{\rho}^\mu - 2g_\rho \boldsymbol{\rho}^\mu \times \boldsymbol{\rho}^\nu \\
F^{\mu\nu} \ = \ \partial^\mu A^\nu \ - \ \partial^\nu A^\mu
\end{cases}
\tag{2}
$$

and other symbols have their usual meanings [1–3].

The classical variation principle leads to the Dirac equation,

$$
\{-\mathrm{i}\boldsymbol{\alpha}\cdot \nabla + V(\boldsymbol{r}) + \beta[M + S(\boldsymbol{r})]\}\psi_i = \epsilon_i \psi_i
\tag{3}
$$

for the nucleon spinors and the Klein–Gordon equations,

$$
\begin{cases}
[-\Delta + m_\sigma^2]\sigma(\boldsymbol{r}) & = \ -g_\sigma \rho_s(\boldsymbol{r}) - g_2 \sigma^2(\boldsymbol{r}) - g_3 \sigma^3(\boldsymbol{r}) \\
[-\Delta + m_\omega^2]\omega^\mu(\boldsymbol{r}) & = \ g_\omega j^\mu(\boldsymbol{r}) - g_4(\omega^\nu \omega_\nu)\omega^\mu(\boldsymbol{r}) \\
[-\Delta + m_\rho^2]\rho^\mu(\boldsymbol{r}) & = \ g_\rho j^\mu(\boldsymbol{r}) \\
-\Delta A^\mu(\boldsymbol{r}) & = \ e j_p^\mu(\boldsymbol{r})
\end{cases}
\tag{4}
$$

for the mesons, where

$$
\begin{cases}
V(\boldsymbol{r}) = \ \beta\Big[g_\omega \gamma^\mu \omega_\mu(\boldsymbol{r}) + g_\rho \gamma^\mu \boldsymbol{\tau}\cdot \boldsymbol{\rho}_\mu(\boldsymbol{r}) + e\gamma^\mu \frac{1-\tau_3}{2}A_\mu(\boldsymbol{r})\Big] \\
S(\boldsymbol{r}) = \ g_\sigma \sigma(\boldsymbol{r})
\end{cases}
\tag{5}
$$

are the vector and scalar potentials, respectively, and the source terms for the mesons and the photons are

$$
\begin{cases}
\rho_s(\boldsymbol{r}) &= \sum\limits_{i=1}^{A} \bar{\psi}_i \psi_i \\
j^\mu(\boldsymbol{r}) &= \sum\limits_{i=1}^{A} \bar{\psi}_i \gamma^\mu \psi_i \\
\boldsymbol{j}^\mu(\boldsymbol{r}) &= \sum\limits_{i=1}^{A} \bar{\psi}_i \gamma^\mu \boldsymbol{\tau} \psi_i \\
j_p^\mu(\boldsymbol{r}) &= \sum\limits_{i=1}^{A} \bar{\psi}_i \gamma^\mu \frac{1-\tau_3}{2} \psi_i
\end{cases}
\tag{6}
$$

In Eq. (6), the summations were taken over the valence nucleons only; that is, no-sea approximation is adopted. The coupled equations [Eqs. (3) and (4)] are nonlinear quantum field equations, and their solutions are very complicated. Therefore, the mean field approximation is generally used to solve Eqs. (3) and (4): that is, the meson field operators in Eq. (4) are replaced by their corresponding expectation values, and the nucleons are considered to move independently in the classical meson fields. In such a way, the said coupled equations can be self-consistently solved by iteration.

The symmetries of the system simplify the calculations considerably. In the system considered in this work, as there exists time reversal symmetry, there are no currents in the nucleus and the spatial vector components of ω, ρ, and A vanish. This leaves only the time-like components ω^0, ρ^0, and A^0. Charge conservation guarantees that only the 3-component of the isovector $\boldsymbol{\rho}$ survives. For simplicity, we denote it in the following simply by ρ^0.

For axially deformed nuclei, i.e., the systems which have rotational symmetry around a symmetrical axis (assumed to be the z-axis), it is useful to work with cylindrical coordinates: $x = r_\perp \cos\varphi$, $y = r_\perp \sin\varphi$, and z. The potential of the nucleon and the sources of meson fields depend only on the coordinates $r_\perp$ and z. The Dirac spinor ψ_i for the nucleon with the index i is characterized by the quantum numbers Ω_i, π_i, and t_i, where $\Omega_i = m_{l_i} + m_{s_i}$ is the eigenvalue of the angular momentum operator J_z, π_i is the parity, and t_i is the isospin; that is, the Dirac spinor ψ_i has the form [18],

$$
\psi_i = \begin{pmatrix} f_i(\boldsymbol{r}) \\ ig_i(\boldsymbol{r}) \end{pmatrix} = \frac{1}{\sqrt{2\pi}} \begin{pmatrix} f_i^+(z,r_\perp)e^{i(\Omega_i-1/2)\varphi} \\ f_i^-(z,r_\perp)e^{i(\Omega_i+1/2)\varphi} \\ ig_i^+(z,r_\perp)e^{i(\Omega_i-1/2)\varphi} \\ ig_i^-(z,r_\perp)e^{i(\Omega_i+1/2)\varphi} \end{pmatrix} \chi_{t_i}(t)
\tag{7}
$$

For each solution with positive Ω_i, ψ_i, there is the time-reversed solution with the same energy, $\psi_{\bar{i}} = T\psi_i$, in which the time reversal operator $T = -i\sigma_y K$ and K is the complex conjugation. For nuclei with time reversal symmetry, the contributions to the densities of the time reversal

states, i and $\bar{i}$, are identical. Therefore, the densities can be represented as

$$
\rho_{s,v} = 2\sum_{i>0} n_i \left[\left(|f_i^+|^2 + |f_i^-|^2 \right) \mp \left(|g_i^+|^2 + |g_i^-|^2 \right) \right]
\tag{8}
$$

and, in a similar way, ρ_3 and ρ_c. The sum here runs over only states with positive Ω_i. The occupation number for state i is represented by n_i. These densities serve as the sources for the fields $\phi = \sigma$, ω^0, ρ^0, and A^0, which are determined by the Klein–Gordon equation in cylindrical coordinates.

To solve Eqs. (3) and (4), the spinors $f_i^\pm(z,r_\perp)$ and $g_i^\pm(z,r_\perp)$ can be expanded in terms of the eigenfunctions of a deformed axially symmetric oscillator potential [18] or Woods–Saxon potential [44], and the solution of the problem is transformed into a diagonalization of a Hermitian matrix. The details can be found in [18,44].

The total energy of the system is:

$$
E_{\mathrm{RMF}} = E_{\mathrm{nucleon}} + E_\sigma + E_\omega + E_\rho + E_c + E_{\mathrm{CM}}
\tag{9}
$$

with

$$
\begin{cases}
E_{\mathrm{nucleon}} &= \sum\limits_i \epsilon_i \\
E_\sigma &= -\frac{1}{2}\int d^3r \left\{ g_\sigma \rho_s(\boldsymbol{r})\sigma(\boldsymbol{r}) + \left[\frac{1}{3}g_2\sigma(\boldsymbol{r})^3 + \frac{1}{2}g_3\sigma(\boldsymbol{r})^4 \right] \right\} \\
E_\omega &= -\frac{1}{2}\int d^3r \left\{ g_\omega \rho_v(\boldsymbol{r})\omega^0(\boldsymbol{r}) - \frac{1}{2}g_4\omega^0(\boldsymbol{r})^4 \right\} \\
E_\rho &= -\frac{1}{2}\int d^3r\, g_\rho \rho_3(\boldsymbol{r})\rho^{00}(\boldsymbol{r}) \\
E_c &= -\frac{e^2}{8\pi}\int d^3r\, \rho_c(\boldsymbol{r})A^0(\boldsymbol{r}) \\
E_{\mathrm{CM}} &= -\frac{3}{4}41A^{-1/3}
\end{cases}
$$

where E_{nucleon} is the sum of the energy for nucleon ε_i, E_σ, E_ω, E_ρ, and E_c are the contributions of the meson fields and the Coulomb field, and E_{CM} is the center of mass correction.

2.2 SLAP for the pairing correlations

Based on the single-particle levels and wave functions obtained from the RMF theory, the SLAP can be adopted to treat the nuclear pairing correlations, hereafter referred as RMF+SLAP. The Hamiltonian reads:

$$
H = H_{\mathrm{s.p.}} + H_{\mathrm{pair}}
\tag{10}
$$

where $H_{\mathrm{s.p.}} = \sum\limits_\nu \varepsilon_\nu a_\nu^+ a_\nu$ and $H_{\mathrm{pair}} = -G \sum\limits_{\mu,\nu>0}^{\mu\neq\nu} a_\mu^+ a_{\bar{\mu}}^+ a_{\bar{\nu}} a_\nu$

with ε_ν the single-particle energy obtained from the RMF theory and H_{pair} the pairing Hamiltonian with average strength G simplified from the quantization of the meson

fields, ν is the notation of the level with the quantum numbers (Ω, π, t) for axially deformed nuclei, and $\bar{\nu}$ is the time-reversal state of ν.

The MPCs are constructed as bases to diagonalize the Hamiltonian in Eq. (10). For an even $N = 2n$ particle system, the MPCs are constructed as the following:

(a) The fully paired configuration (seniority $s = 0$):

$$|\rho_1 \bar{\rho}_1 \cdots \rho_n \bar{\rho}_n\rangle = a_{\rho_1}^+ a_{\bar{\rho}_1}^+ \cdots a_{\rho_n}^+ a_{\bar{\rho}_n}^+ |0\rangle \qquad (11)$$

(b) The configuration with two unpaired particles (seniority $s = 2$):

$$\begin{aligned}
&|\mu \bar{\nu} \rho_1 \bar{\rho}_1 \cdots \rho_{n-1} \bar{\rho}_{n-1}\rangle \\
&= a_\mu^+ a_{\bar{\nu}}^+ a_{\rho_1}^+ a_{\bar{\rho}_1}^+ \cdots a_{\rho_{n-1}}^+ a_{\bar{\rho}_{n-1}}^+ |0\rangle,
\end{aligned} \qquad (12)$$

and so on [34]. The MPC for an odd $N = 2n + 1$ particle system can be constructed similarly. For the axially deformed nuclei, as the parity π, seniority s, and eigenvalue K of the third component for the total angular momentum operator J_z are good quantum numbers, the MPC space of an even particle system can be written as the following:

MPC space
$$\begin{aligned}
= &(s = 0, K = 0^+) \oplus (s = 2, K = 0^+) \\
&\oplus (s = 2, K = 1^+) \oplus (s = 2, K = 2^+) \oplus \cdots \\
&\oplus (s = 4, K = 0^+) \oplus (s = 4, K = 1^+) \\
&\oplus (s = 4, K = 2^+) \oplus \cdots \oplus \cdots
\end{aligned} \qquad (13)$$

In realistic calculation, the MPC space has to be truncated and an energy cutoff E_c is introduced. Only the configurations with energies $E_i - E_0 \leqslant E_c$ are used to diagonalize the Hamiltonian H in Eq. (10), where E_i and E_0 are the energies of the ith configuration and the lowest configuration, respectively. The cutoff in the single-particle states is implicitly included in the energy cutoff E_c.

The corresponding nuclear wave function can be expanded as

$$\begin{aligned}
\psi^\beta = &\sum_{\rho_1, \cdots, \rho_n} V_{\rho_1, \cdots, \rho_n}^\beta |\rho_1 \bar{\rho}_1 \cdots \rho_n \bar{\rho}_n\rangle \\
&+ \sum_{\mu, \nu} \sum_{\rho_1, \cdots, \rho_{n-1}} V_{\rho_1, \cdots, \rho_{n-1}}^{\beta(\mu\nu)} |\mu \bar{\nu} \rho_1 \bar{\rho}_1 \cdots \rho_{n-1} \bar{\rho}_{n-1}\rangle + \cdots
\end{aligned} \qquad (14)$$

where $\beta = 0$ (ground state), 1, 2, 3, ... (excited states).

The occupation probability of the ith level for state β is

$$\begin{aligned}
n_i^\beta = &\sum_{\rho_1, \cdots, \rho_{n-1}} \left| V_{\rho_1, \cdots, \rho_{n-1}, i}^\beta \right|^2 + \sum_{\mu, \nu} \sum_{\rho_1, \cdots, \rho_{n-2}} \left| V_{\rho_1, \cdots, \rho_{n-2}, i}^{\beta(\mu\nu)} \right|^2 \\
&+ \cdots, \quad i = 1, 2, 3, \cdots
\end{aligned}$$

$$(15)$$

Replacing the occupation number n_i in Eq. (8) by $n_i^{\beta=0}$, the sources in Eq. (4) are obtained and the occupancies thus obtained have been iterated back into the densities, which give new meson fields and a new electromagnetic field. These new fields then are used to calculate the vector and scalar potentials in Eq. (5). With these new potentials, the Dirac equation [Eq. (3)] is solved again. These processes should be repeated until the results converge to the given precision. As the pairing correlations are taken into account, the pairing energy $E_{\text{pair}} = \langle \psi^\beta | H_{\text{pair}} | \psi^\beta \rangle$ should be added to the total energy in Eq. (9).

3 Results and discussions

We have performed the RMF+SLAP calculations for the Ne isotopes with the usual effective interactions, e.g., PK1 [45], NLSH [46], NL3 [47], and TMA [48]. As the conclusions do not depend on the effective interactions used here, only the results with the effective interaction PK1 are presented in detail. A similar investigation has been done with the RMF+BCS approach in [49]. For the axially deformed nuclei, the parity π and the eigenvalue K of the third component of total angular momentum operator J_z are good quantum numbers. In the numerical calculations, the Dirac equation [Eq. (3)] for the nucleons and the Klein–Gordon equations [Eq. (4)] for the mesons and the photon are solved by expansion in the harmonic oscillator basis with 14 oscillator shells for both the fermion fields and the boson fields. The oscillator frequency of the harmonic oscillator basis is fixed as $\hbar\omega_0 = 41A^{-1/3}$ MeV and the deformation of harmonic oscillator basis β_0 is reasonably set to obtain the lowest energy.

Taking ^{24}Ne as an example, the detailed procedures of SLAP for the pairing correlations are the following:

- From the solution of the Dirac equation, the neutron and proton single-particle levels are obtained, as schematically shown in Fig. 1, where the dashed line represents the last occupied level in the filling approximation.
- With the single-particle levels thus obtained, the MPC are constructed according to Eqs. (11) and (12) (see also [34]) with given truncation energy E_c. The truncation energy E_c is chosen in such a way that no configurations with important weights are omitted in the SLAP calculations. In the following calculations on the Ne isotopes, the truncation energy is reasonably fixed to $E_c = 40$ MeV. With this truncation energy, all the configurations with weight above 3.7×10^{-6} have been included for ^{24}Ne, while configurations with
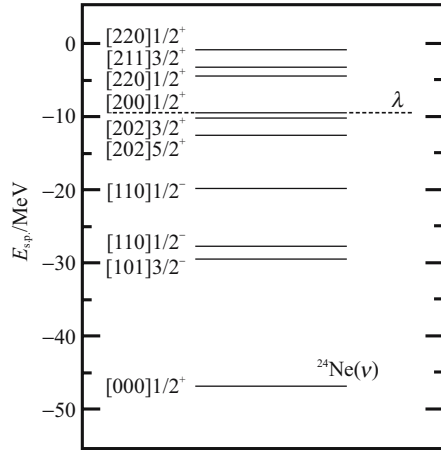
Fig. 1 The neutron single-particle levels in ^{24}Ne in RMF with PK1. The *dashed line* represents the Fermi surface λ, which is also the last occupied orbit in the simple filling approximation

weight above 0.032% have been included for ^{18}Ne. More detailed discussion on the configuration truncation can be found in [34,35,38,39–43] and references therein.

- As the parity π, seniority s, and K are good quantum numbers, the Hamiltonian H in Eq. (10) is block diagonal in the MPC space Eq. (13). In every subspace, the single-particle Hamiltonian $H_{s.p.}$ is diagonal. The nonzero off-diagonal matrix elements come from H_{pair} for configurations with a difference of one-pair particles in the particle-pair occupation orbital. The pairing strength $G_\tau = C_\tau/A$ MeV ($\tau = p, n$) is adopted for all the Ne isotopes, as normally done in RMF+BCS calculations, e.g., see [50]. Here, for truncation energy $E_c = 40$ MeV, $C_\tau = 10$ is fixed by reproducing the experimental odd–even mass difference of $^{24-26}$Ne.
- By diagonalizing the matrix of the Hamiltonian H in Eq. (10) obtained above, the solutions for the ground state and the low-lying excited states are obtained. The occupation probabilities n_i^β of the single-particle level i in state β can be calculated from Eq. (15). Replacing the occupation number n_i by $n_i^{\beta=0}$ in Eq. (8), the densities in Eq. (6) can be obtained, which give the new meson fields and a new electromagnetic field. These new fields can be used to calculate the vector and scalar potentials in Eq. (5). With these new vector and scalar potentials, the Dirac equation [Eq. (3)] is solved again.

- The above processes should be repeated until the results converge to the given precision. The calculated results obtained in such a way will be referred as RMF+SLAP in the following.

As the pairing correlations are taken into account, for state β, the energy for nucleons $E_{nucleon}$ in the total energy of system Eq. (9) should be modified as:

$$E_{nucleon} = \sum_i n_i^\beta \varepsilon_i$$

and the pairing energy $E_{pair} = \langle \psi^\beta | H_{pair} | \psi^\beta \rangle$ should be added to the total energy.

The results for the ground state of ^{24}Ne from the RMF+SLAP* and RMF+SLAP calculations with PK1 are shown in Table 1, including the binding energy E, binding energy per nucleon E/A, the root mean square (rms) radii for neutron, proton, and matter, R_n, R_p, and R_m, and the quadrupole deformation for neutron, proton, and matter, β_{2n}, β_{2p}, and β_{2m}. The difference between these two calculations lies in that in RMF+SLAP*, the occupancies obtained by SLAP is not iterated back into the densities. While in RMF+SLAP, the occupancies obtained by SLAP are self-consistently iterated back into the densities. The corresponding calculations and the data available [51,52] are included for comparisons. From Table 1, it can be seen that as pairing correlations are taken into account, both the RMF+SLAP* and RMF+SLAP calculations provide more binding for the total binding energy and larger rms radii due to the contribution from those loosely bound levels, which is similar as that obtained from the Bogoliubov transformation, i.e., the pairing correlations can increase the nuclear rms radius [8]. However, compared with RMF+SLAP*, the binding energy from RMF+SLAP calculations is less. Furthermore, the deformation of nucleus reduced by the pairing correlations is realized only in RMF+SLAP, which clearly demonstrated the necessity to iterate the occupancies obtained by SLAP self-consistently back into the densities.

As the Pauli blocking effects can be strictly treated in SLAP, a self-consistent description for even–even, odd–A, and odd–odd nuclei can be obtained in the RMF+SLAP calculations. In Fig. 2, the occupation probabilities for the neutron levels are displayed for ^{24}Ne in the left panel and for ^{25}Ne in the right panel, where the occupation prob-

Table 1 The binding energy, radii, and deformation of ground state in ^{24}Ne obtained from the RMF+SLAP* and RMF+SLAP calculations with PK1, in comparison with the RMF calculation and data available

	E	E/A	R_n	R_p	R_m	β_{2n}	β_{2p}	β_{2m}
EXP	−191.836	−7.993						−0.45
RMF	−189.283	−7.887	2.985	2.756	2.892	−0.278	−0.238	−0.261
RMF+SLAP*	−190.723	−7.947	2.994	2.757	2.898	−0.278	−0.236	−0.261
RMF+SLAP	−189.974	−7.916	2.994	2.758	2.898	−0.275	−0.235	−0.258

Total binding energy E, binding energy per nucleon E/A, neutron, proton, and matter rms radii, R_n, R_p, and R_m, and the quadrupole deformation parameters for the neutron, proton, and matter distributions, β_{2n}, β_{2p}, and β_{2m}, respectively are listed.

Fig. 2 The occupation probabilities for the neutron single-particle levels in ^{24}Ne and ^{25}Ne obtained from RMF+SLAP calculation with PK1, where the occupation probabilities of levels above [202]5/2$^+$ for ^{24}Ne and those of levels above [200]1/2$^+$ for ^{25}Ne are multiplied by a factor of 10 for clarity
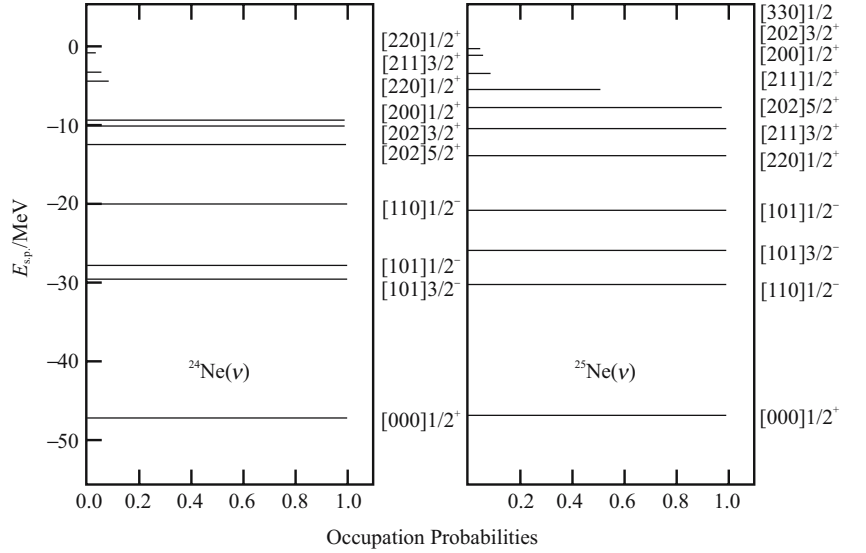
abilities of levels above [202]5/2$^+$ for ^{24}Ne and those of levels above [200]1/2$^+$ for ^{25}Ne are multiplied by a factor of 10 for clarity. For ^{24}Ne, if without pairing correlation, the levels above [202]5/2$^+$ will be unoccupied and the others are fully occupied. In the RMF+SLAP calculations, the levels above [202]5/2$^+$ have been occupied partly, while the occupation probabilities for levels below Fermi surface are decreased accordingly. For ^{25}Ne, [200]1/2$^+$ is the blocking level and is occupied by a single nucleon in the RMF+SLAP calculations. The occupations for the levels beyond [200]1/2$^+$ have been reduced due to the blocking effects. For ^{24}Ne, both RMF+SLAP* and RMF+SLAP calculations have been done, and it turned out that their difference in the occupation probabilities can be neglected.

The ground state properties of Ne isotopes including the odd–A and even–even nuclei from the RMF+SLAP calculations with PK1 are listed in Table 2, including the total binding energy E, the binding energy per nucleon E/A,

the rms radii for neutron, proton, and matter, R_n, R_p, and R_m, and the quadrupole deformation for neutron, proton, and matter, β_{2n}, β_{2p}, and β_{2m}. The binding energies per nucleon for Ne isotopes from the RMF+SLAP calculations are shown in Fig. 3, in comparison with the available data [51]. It can be seen that for the ground state, the RMF+SLAP calculations, which are similar with the RMF+BCS calculations [49], give a very good description of the data, except for the proton-rich nucleus ^{18}Ne. However, RMF+SLAP approximation can do more than RMF+BCS calculations, as will be seen in the following.

One- and two-neutron separation energies defined as

$$S_n(Z, N) = E(Z, N) - E(Z, N - 1) \tag{16}$$

and

$$S_{2n}(Z, N) = E(Z, N) - E(Z, N - 2) \tag{17}$$

Table 2 The ground state properties of Ne isotopes obtained from the RMF+SLAP calculations with PK1, including the binding energy E, binding energy per nucleon E/A, neutron, proton, and matter rms radii, R_n, R_p, and R_m, and the quadrupole deformation parameters for the neutron, proton, and matter distributions, β_{2n}, β_{2p} and β_{2m}, respectively, with A the mass number and N the neutron number

| A	N	E	E/A	R_n	R_p	R_m	β_{2n}	β_{2p}	β_{2m}
18	8	−135.584	−7.532	2.555	2.951	2.782	0.000	0.035	0.020
19	9	−144.546	−7.608	2.686	2.840	2.768	0.312	0.434	0.377
20	10	−157.932	−7.897	2.805	2.839	2.822	0.518	0.533	0.526
21	11	−166.982	−7.952	2.867	2.823	2.846	0.513	0.507	0.510
22	12	−176.806	−8.037	2.928	2.813	2.876	0.508	0.487	0.499
23	13	−182.704	−7.944	2.958	2.789	2.885	0.368	0.408	0.386
24	14	−189.974	−7.916	2.994	2.758	2.898	−0.275	−0.235	−0.258
25	15	−194.881	−7.795	3.088	2.786	2.971	0.256	0.326	0.284
26	16	−200.902	−7.727	3.180	2.807	3.042	0.277	0.327	0.296
27	17	−204.405	−7.570	3.253	2.821	3.100	0.224	0.306	0.254
28	18	−209.152	−7.470	3.333	2.836	3.165	0.191	0.289	0.226
29	19	−211.688	−7.300	3.376	2.850	3.205	0.117	0.234	0.157
30	20	−215.708	−7.190	3.428	2.863	3.251	0.055	0.160	0.090
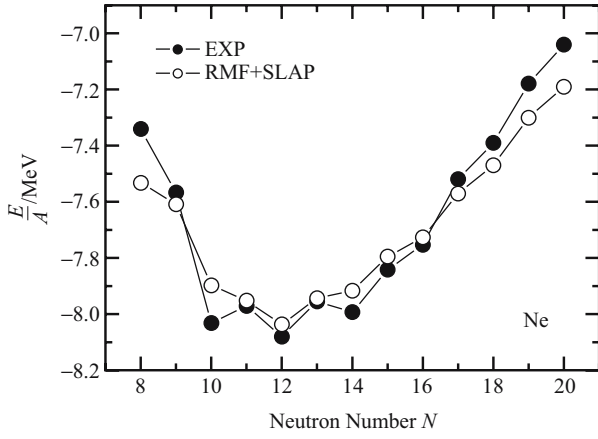
Fig. 3 Binding energy per nucleon, E/A, for Ne isotopes as functions of neutron number N obtained from the RMF+SLAP calculations (*filled circles*) with PK1 in comparison with the data (*open circles*)

Fig. 5 Quadrupole deformation, β_2, for Ne isotopes as functions of neutron number N obtained from the RMF+SLAP calculations (*filled circles*) with PK1 in comparison with the data (*open circles*)

are sensitive quantities to test a microscopic theory, where $E(Z, N)$ is the binding energy of nucleus with proton number Z and neutron number N.

In Fig. 4, the one- and two-neutron separation energies from the RMF+SLAP calculations (filled circles) with PK1 in comparison with the data (open circles) are shown [51]. From the figure, it can be seen that the experimental odd–even staggering is well reproduced in the RMF+SLAP calculations for either the one-neutron separation energy or the two-neutron separation energy.

In Fig. 5, the deformations β_2 for Ne isotopes from the RMF+SLAP calculations are given, including the data [52]. It should be mentioned that as the prolate or oblate shapes cannot be distinguished experimentally, the assumption of shape oblate for ^{24}Ne has been done. First of all, the tendency for the shape change with neutron number in Ne isotopes is correctly reproduced. The RMF+SLAP calculations give even better results than the RMF+BCS
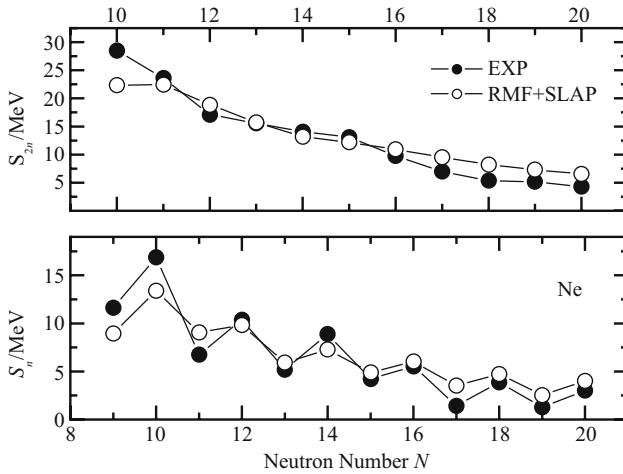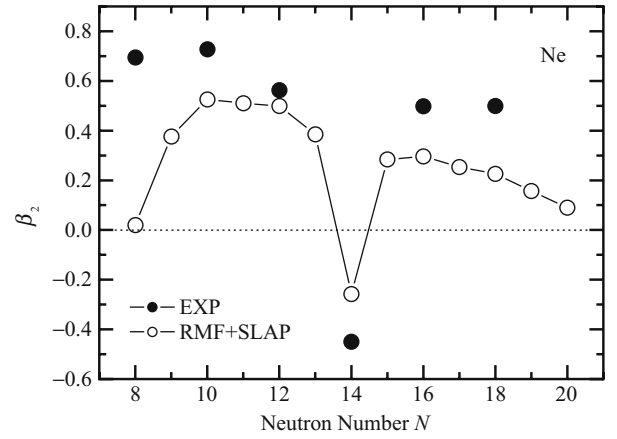
calculations [49]. From the figure, it can be seen that the deformations are generally underestimated, particularly for the proton-rich side. In [53], the deformation parameter β is determined from $B(E2) \uparrow$ for the ground state to 2^+ state

$$\beta = (4\pi/3ZR_0^2)[B(E2) \uparrow /e^2]^{1/2} \tag{18}$$

where the radius R_0 has been taken to be $1.2A^{1/3}$ fm. However, it has been well demonstrated that the experiential relation of radius is only suitable for medium-mass and heavy nuclei [53]. While for light nuclei, the estimation for the radius R_0 is too small, which leads to a large deformation β with Eq. (18). With this factor considered, the consistency between the calculation results and the deformation data will be more agreeable.

The neutron, proton, and total pairing energies from the RMF+SLAP calculations are displayed in Fig. 6 as open circles, open squares, and filled circles, respectively. It can be seen that the odd–even staggering has been clearly
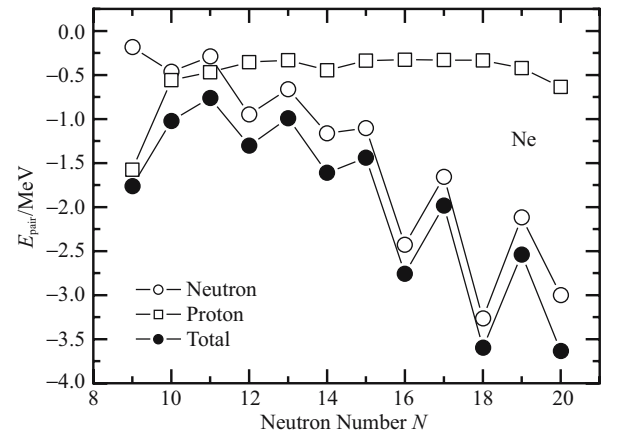

Fig. 4 One- and two-neutron separation energies, S_n and S_{2n}, for Ne isotopes as functions of neutron number N obtained from the RMF+SLAP calculations (*filled circles*) with PK1 in comparison with the data (*open circles*)

Fig. 6 Pairing energies, E_{pair}, obtained from the RMF+SLAP calculations with PK1 for Ne isotopes as functions of neutron number N for neutron (*open circles*), proton (*open squares*), and total nuclear matter (*filled circles*)
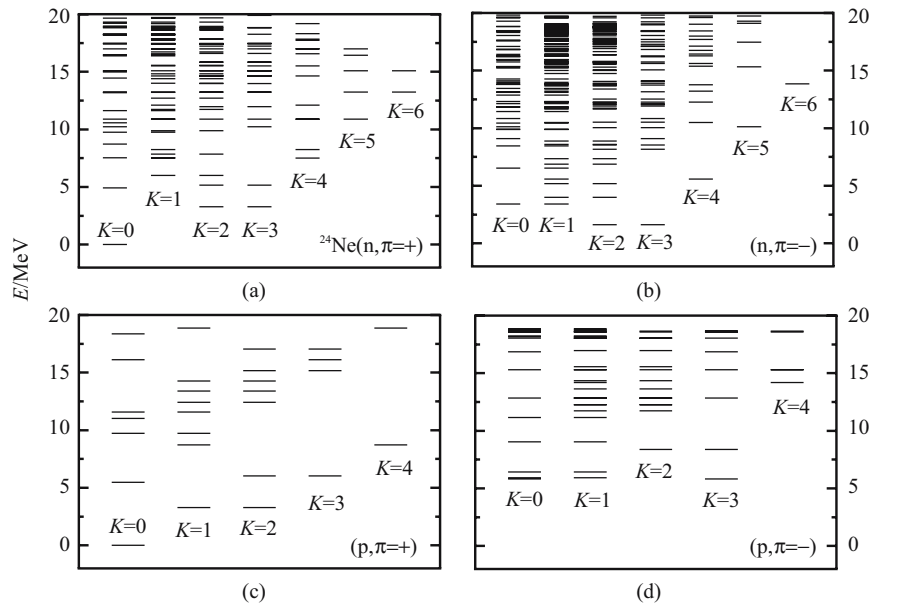
revealed for the neutron pairing energy due to the correct treatment of the Pauli blocking effects, while the proton pairing energy varies smoothly with the neutron number N. The large neutron pairing energy at $N = 20$ in present calculations indicates disappearances of the traditional magic number at $N = 20$ in the Ne isotope chain. Although from Fig. 5 the nucleus ^{30}Ne is nearly spherical ($\beta_2 \sim 0.1$), the magic number $N = 20$ disappears. This indicates that the disappearance of the magic number here is not due to the deformation; instead, it might be due to the fact that the neutron Fermi surface in ^{30}Ne is very close to the threshold of continuum, as noted and discussed in [4,54,55].

To justify the description for nuclei close to the drip line, one should adopt the analytical continuation in coupling constant (ACCC) method or the S-matrix method [22,24,25] to re-sort the resonance states. Studies along this line are in progress.

The unified description for both the ground and excited states is another advantage of the RMF+SLAP. By diagonalization of the pairing Hamiltonian in the corresponding subspace with fixed K, parity π, and seniority s, the spectra of multiparticle collective excitations can be obtained.

As an example, the collective excitation spectra for ^{24}Ne are shown in Fig. 7, where panels a, b, c, and d, respectively, represent the spectra of positive and negative parity for neutron and those for proton. The calculated 0^+ excitation spectra include $E_n^{0^+}$ =5.622 MeV for neutron and $E_p^{0^+}$ =4.912 MeV for proton, which are very close to the only known experimental data $E_{\exp}^{0^+}$ =4.764 MeV. From Fig. 7, it can also be seen that the RMF+SLAP can also be used to investigate the excited states with high-K value. It may provide another self-consistent microscopic description and prediction of the interesting high-K energy trap [56,57].

4 Summary

The SLAP has been applied to treat the pairing correlations in the framework of RMF theory, which can exactly treat the Pauli blocking effects. The formalism and numerical techniques are presented in detail, and the Ne isotopes are taken as an example to demonstrate the applicability of the method.

First of all, the RMF+SLAP with effective interaction PK1 has been used to describe the ground state properties of the Ne isotopes, including the binding energies, one-neutron and two-neutron separation energies, deformation, pairing energy and occupation probability of single-particle orbital, etc. The calculated binding energies from the RMF+SLAP agree well with the data and are comparable with the RMF+BCS calculations. The odd–even staggering is well reproduced, as shown in the neutron pairing energy and one-neutron or two-neutron separation energies. The tendency for the change of the shapes with neutron number in Ne isotopes is correctly reproduced. Furthermore, the RMF+SLAP calculations give better results than the RMF+BCS calculations for ^{26}Ne and ^{28}Ne.

The other advantage of the RMF+SLAP method is the description of both the ground and excited states simultaneously. As examples, the collective excitation spectra for ^{24}Ne with positive and negative parity for both proton and neutron are presented. Its potential application for the interesting high-K energy trap has been demonstrated.

In conclusion, SLAP is a good method to treat the pairing correlations in the RMF theory, which can provide a good description for the properties not only in the ground state but also in the excited states.

Fig. 7 The excitation spectra obtained from the RMF+SLAP calculations with TMA in ^{24}Ne. The quantum number K is the eigenvalue for the third component of the total angular momentum operator J_z. (**a**), (**b**), (**c**), and (**d**), respectively, represent the spectra of positive and negative parity for neutron and proton

References

1. Serot B. -D. and Walecka J. -D., Adv. Nucl. Phys., 1986, 16: 1
2. Reinhard P. -G., Rep. Prog. Phys., 1989, 52: 439
3. Ring P., Prog. Part. Nucl. Phys., 1996, 37: 193
4. Meng J., Nucl. Phys., A, 1998, 635: 3
5. Meng J., Toki H., Zhou S. -G., Zhang S. -Q., Long W. -H., Geng L. -S., Prog. Part. Nucl. Phys., 2005 (in press)
6. Brockmann R. and Machleidt R., Phys. Rev., C, 1990, 42: 1965
7. König J. and Ring P., Phys. Rev. Lett., 1993, 71: 3079
8. Meng J. and Ring P., Phys. Rev. Lett., 1996, 77: 3963
9. Meng J. and Ring P., Phys. Rev. Lett., 1998, 80: 460
10. Arima A., Harvey M. and Shimizu K., Phys. Lett., Sect. B, 1969, 30: 517
11. Hecht K. -T. and Adler A., Nucl. Phys., A, 1969, 137: 129
12. Ginocchio J. N., Phys. Rev. Lett., 1997, 78: 436
13. Meng J., Sugawara-Tanabe K., Yamaji S., Ring P. and Arima A., Phys. Rev., C, 1998, 58: R628
14. Meng J., Sugawara-Tanabe K., Yamaji S. and Arima A., Phys. Rev., C, 1999, 59: 154
15. Zhou S. -G., Meng J. and Ring P., Phys. Rev. Lett., 2003, 91: 262501
16. Madokoro H., Meng J., Matsuzaki M. and Yamaji S., Phys. Rev., C, 2000, 62: 061301
17. Ma Z. -Y., Wandelt A., Giai N. -V., Vretenar D., Ring P. and Cao L. -G., Nucl. Phys., A, 2002, 703: 222
18. Gambhir Y. -K. and Ring P., Thimet A., Ann. Phys. (N.Y.), 1990, 198: 132
19. Geng L. -S., Toki H., Sugimoto S. and Meng J., Prog. Theor. Phys., 2003, 110: 921
20. Dobaczewski J., Flocard H. and Treiner J., Nucl. Phys., A, 1984, 422: 103
21. Dobaczewski J., Nazarewicz W., Werner T. R. et al., Phys. Rev., C, 1996, 53: 2809
22. Yang S. -C., Meng J. and Zhou S. -G., Chin. Phys. Lett., 2001, 18: 196
23. Cao L. -G. and Ma Z. -Y., Phys. Rev., C, 2002, 66: 024311
24. Sandulescu N., Geng L. -S., Toki H. and Hillhouse G., Phys. Rev., C, 2003, 68: 054323
25. Zhang S. -S., Meng J., Zhou S. -G. and Hillhouse G. -C., Phys. Rev., C, 2004, 70: 034308
26. Peierls R. -E. and Yoccoz J., Proc. Phys. Soc., 1957, A70: 381
27. Ring P. and Schuck P., The Nuclear Many-Body Problem, Berlin Heidelberg New York: Springer, 1980
28. Zeh H. -D., Z. Phys., 1967, 202: 38
29. Hara K. and Sun Y., Int. J. Mod. Phys., 1995, E4: 637
30. Egido J. -L. and Ring P., Nucl. Phys., 1982, A383: 189
31. Egido J. -L. and Ring P., Nucl. Phys., 1982, A388: 19
32. Sheikh J. -A. and Ring P., Nucl. Phys., 2000, A665: 71
33. Sheikh J. -A., Ring P., Lopes E. and Rossignoli R., Phys. Rev., C, 2002, 66: 044318
34. Zeng J. -Y. and Cheng T. -S., Nucl. Phys., A, 1983, 405: 1
35. Zeng J. -Y., Lei Y. -A., Jin T. -H. and Zhao Z. -J., Phys. Rev., C, 1994, 50: 746
36. Rowe D. -J., Nuclear Collective Motion, London: Methuen, 1970
37. Chasman R. R., Phys. Lett., Sect. B, 1990, 242: 317
38. Molique H. and Dudek J., Phys. Rev., C, 1997, 56: 1795
39. Wu C. -S. and Zeng J. -Y., Phys. Rev., C, 1989, 39: 666
40. Wu C. -S. and Zeng J. -Y., Phys. Rev. Lett., 1991, 66: 1022
41. Zeng J. -Y., Jin T. -H. and Zhao Z. -J., Phys. Rev., 1994, 50: 1388
42. Zeng J. -Y., Liu S. -X., Lei Y. -A. and Yu L., Phys. Rev., C, 2001, 63: 024305
43. Zeng J. -Y., Liu S. -X., Gong L. -X. and Zhu H. -B., Phys. Rev., C, 2002, 65: 044307
44. Zhou S. -G., Meng J. and Ring P., Phys. Rev., C, 2003, 68: 034323
45. Long W. -H., Meng J., Giai N. -V. and Zhou S. -G., Phys. Rev., C, 2004, 69: 034319
46. Sharma M., Nagarajan M. and Ring P., Phys. Lett., Sect. B, 1993, 312: 377
47. Lalazissis G. -A., König J. and Ring P., Phys. Rev., C, 1997, 55: 540
48. Sugahara Y., Doctoral Thesis, Tokyo Metropolitan University, 1995
49. Geng L. -S., Toki H., Ozawa A. and Meng J., Nucl. Phys., A, 2004, 730: 80
50. Del Estal M., Centelles M., Viñas X. and Patra S. -K., Phys. Rev., C, 2001, 63: 044321
51. Audi G. and Wapstra A. -H., Nucl. Phys., A, 1995, 595: 409
52. Raman S., Nestor C. -W. Jr. and Tikkanen P., At. Data Nucl. Data Tables, 2001, 78: 1
53. Zhang S. -Q., Meng J., Zhou S. -G. and Zeng J. -Y., Eur. Phys. J., A, 2002, 13: 285 (and references therein)
54. Meng J., Tanihata I. and Yamaji S., Phys. Lett., Sect. B, 1998, 419: 1
55. Meng J., Toki H., Zeng J. -Y., Zhang S. -Q. and Zhou S. -G., Phys. Rev., C, 2002, 65: 041302
56. Baldwin G. -C. and Solem J. -C., Rev. Mod. Phys., 1997, 69: 1085
57. Walker P. -M. and Dracoulis G. -D., Nature, 1999, 399: 35